agriculture

MDPI

Article

Optimization and Experiment of a Disturbance-Assisted Seed Filling High-Speed Vacuum Seed-Metering Device Based on DEM-CFD

Rui Liu [1,2], Zhongjun Liu [2], Jiale Zhao [3], Qi Lu [2], Lijing Liu [1,2,*] and Yinghang Li [4]

[1] College of Engineering, China Agricultural University, Beijing 100083, China
[2] The State Key Laboratory of Soil, Plant and Machine System Technology, Beijing 100083, China
[3] Key Laboratory of Bionic Engineering, Jilin University, Ministry of Education of China, Changchun 130022, China
[4] Modern Agricultural Equipment Co., Ltd., Beijing 100083, China
* Correspondence: liulijing@caams.org.cn; Tel.: +86-136-5138-0575

Abstract: In disturbance-assisted seed filling vacuum seed-metering devices, the suction hole causes difficulty in quickly and stably sucking seeds when used for high-speed seeding and the large working negative pressure demand is used. To address this difficulty, this study's authors designed a seed disk hole with a variable cross-section structure, and the groove depth, which has the function of assisting seed filling, was optimized. Using the combined method of Fluent numerical analysis and an orthogonal experiment, the influence of the shape, inlet diameter, and length of the seed disk hole on the pressure difference of the seed disk hole was analyzed. The working process of the vacuum seed meter was simulated and analyzed by the Discrete Element Method and Computational Fluid Dynamics coupling method. It was found that with the increase of the diameter of the seed disk hole, the pressure difference decreased, and the length of the seed disk hole had little effect on the pressure difference. The best diameter of the seed disk hole was 5.4 mm, and the length was 5 mm. It was found that the pressurization effect of the arc-shaped seed disk hole is better. With the increase of groove depth, the leakage rate shows a trend of first decreasing and then increasing, which was determined to be 1.5 mm. The verification experiment proved that the working performance of the optimized seed metering device is better than that of the original one. The results show that when the working negative pressure was 4 kPa and the working speeds were 8~14 km·h^{-1}, the qualified rate was not less than 95.0%, and the seed filling performance was relatively stable. The optimized vacuum seed metering device can be applied to high-speed seeders, while ensuring the requirements of high-speed sowing operations.

Keywords: airflow field; seed metering device; high-speed precision; simulation analysis; optimal design

check for updates

Citation: Liu, R.; Liu, Z.; Zhao, J.; Lu, Q.; Liu, L.; Li, Y. Optimization and Experiment of a Disturbance-Assisted Seed Filling High-Speed Vacuum Seed-Metering Device Based on DEM-CFD. *Agriculture* **2022**, *12*, 1304. https://doi.org/10.3390/agriculture12091304

Academic Editor: Jacopo Bacenetti

Received: 18 July 2022
Accepted: 10 August 2022
Published: 25 August 2022

Publisher's Note: MDPI stays neutral with regard to jurisdictional claims in published maps and institutional affiliations.

Copyright: © 2022 by the authors. Licensee MDPI, Basel, Switzerland. This article is an open access article distributed under the terms and conditions of the Creative Commons Attribution (CC BY) license (https://creativecommons.org/licenses/by/4.0/).

1. Introduction

Maize is one of the world's most important crops and can be used as an industrial raw material. At present, China's urbanization process is accelerating, and agricultural production labor is in short supply, which affects the yield of maize. In order to adapt to the development of modern agriculture, new seeding technology is urgently needed [1,2]. High-speed precision seeding technology is an engineering technology with remarkable yield-increasing effect. It is characterized by saving seeds, saving labor, and increasing production, which is conducive to promoting the further development of the rural economy [3]. High-performance, high-speed precision seeding equipment is the basis for realizing advanced seeding technology [4–8]. The Vacuum Seed metering device relies on negative pressure to pick up one seed and carry it out of bulk. It is then discharged into a seed tube. At this point, the single hole carrying two or more seeds is defined as multiple seeds, and the single hole carrying zero seeds is defined as missed seeds. When

the airflow passes through the seed disk hole, a part of the pressure will be lost. When the working negative pressure is the same, and the plant distance is 20 cm, with the working speed is 8–14 km/h, the rotational speed of the seed disk increases and the seed filling time decreases, increasing the leakage rate, compared with the operating speed less than 8 km/h. Generally, the qualified seed filling rate can be ensured by increasing the working negative pressure, but at the same time, the fan's energy consumption will be increased [9]. Therefore, it is necessary to improve the structure of the seed disk hole, reduce the pressure loss and make the airflow establish a stable velocity field and pressure field in the seed disk hole to ensure that the adsorption pressure increases when the working negative pressure is the same. At the same time, the auxiliary seed filling structure must be increased to improve the seed-filling performance of the seed metering device.

Researchers have successfully used the two-phase flow coupling method with the combination of the Discrete Element Method (DEM). Computational Fluid Dynamics (CFD) has be used to quantitatively study the particle-breaking process in a jet mill [10], the movement process of airflow transported seeds [11,12], the filling process of the pneumatic seed metering device [13–17], the design of seed feeding devices and horizontal seed supply pipe of the air-assisted centralized metering system [18,19], and it has also been used as a tool for optimizing the design of the machine structure [20–28]. Shi et al. analyzed the main factors affecting the filling performance at each stage of the filling process at a microscopic scale. By using a gas–solid coupling simulation, the seed-metering device was optimized by taking the seed adsorption stabilization time, seed removal resistance and local porosity at the shaped hole as the experiment indices [29]. Ding et al. analyzed the pressure of each area of the seed-metering device based on DEM-CFD gas–solid coupling simulation and designed the air inlet of the seed-metering device [30]. Han et al. used the DEM-CFD gas–solid coupling analysis to conduct simulation experiments with the installation position of the gas nozzle, working negative pressure and forward speed of the machine as the experiment factors to determine the installation structure parameters of the gas nozzle [31]. Given the problem that the Vacuum Seed metering device is prone to miss sowing and suction during high-speed work, the researchers solved the problem by changing the structure and position of the air inlet and adding an auxiliary seed filling structure to the vacuum meter seed disk. However, there are relatively few studies on seed disk holes.

To further improve the seed-filling performance of the disturbance-assisted high-speed maize air-suction seed-metering device, this paper firstly analyzed the airflow field flowing through the seed disk hole with the help of Ansys Fluent 18.0 software (American ANSYS company, which is located in Pittsburgh, PA, USA) and discussed the influence of the structure, length and entrance diameter of the seed disk hole on the pressure difference. Secondly, using the DEM-CFD coupled simulation analysis, the gas–solid two-phase flow simulation was carried out on the migration process of the seeds with the rotation of the seed disk. The effects of operating speed, working negative pressure, and groove depth on seeding performance were specifically studied. The underlying mechanisms were analyzed. Finally, the optimal working parameters of the seed meter were determined and verified by bench experiments. In this study, a new structural improvement method is provided to solve the problem of poor high-speed operation performance of the vacuum seed metering device, which can improve the operation accuracy of the seed metering device.

2. Disturbance-Assisted Seed Filling High-Speed Seed Metering Device

2.1. Overall Structure of Seed Metering Device

The structure model of the disturbance-assisted seed filling high-speed air-suction seed-metering device is shown in Figure 1. The vacuum meter seed disk, upper scraper and lower scraper are the core working components that directly contact the seeds. Their structural parameters directly affect the process of filling, seed-carrying and seeding, ultimately determining whether the seed-metering device can achieve single-seed sowing [2]. The vacuum meter seed disk comprises a "zhong"-shaped seed disk hole, concave groove

teeth, a seed disturbing post and the vacuum meter seed disk body. Please note that when the grooves were dug out on the seed disk, the seed disk hole and the remaining area are similar to the Chinese character "zhong", so it is named the "zhong"-shaped seed disk hole. The diameter of the seed disk is 200 mm, and there are 32 seed disk holes on it. The diameter of the circle where the center of the seed disk holes is located is 120 mm. It is known from the literature [32] that the maximum length of maize seed(L)is 12.82 mm. As shown in Figure 2. To satisfy the smooth entry of a single seed into the groove, the length and width of the groove should be larger than the length and width of the seed. Meanwhile, considering the convenience of making a seed disk, it was determined that r_1 was 67 mm, r_2 was 51 mm, and C was 14 mm.

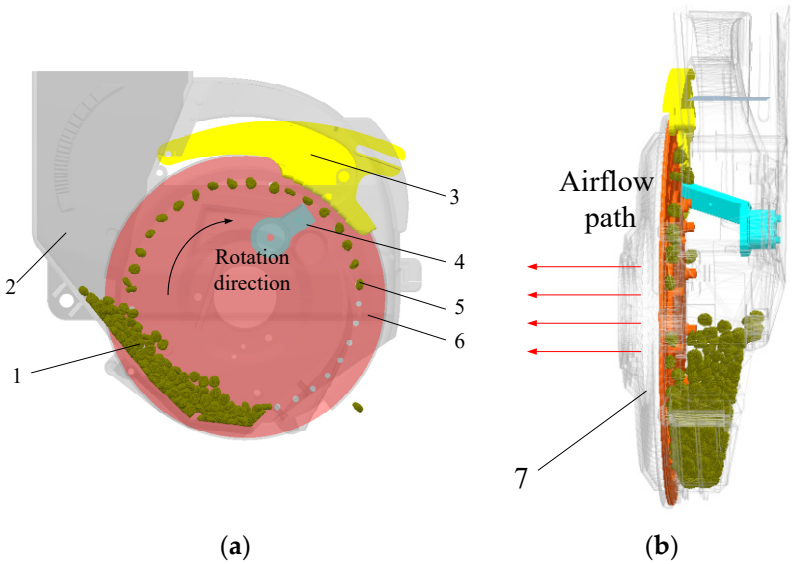

Figure 1. (**a**) Main view (**b**) Left view. Disturbance-assisted seed filling high-speed air-suction seed-metering device model: (1) seed group in seed filling area, (2) seed metering housing, (3) upper scraper, (4) lower scraper, (5) stably adsorbed seeds, (6) vacuum meter seed disk, (7) vacuum chamber.

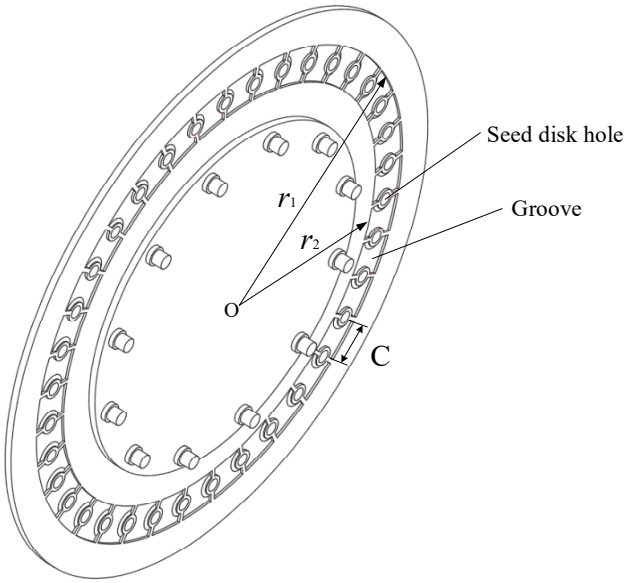

Figure 2. Two-dimensional sketch of the seed disk.

2.2. Working Principles

When the vacuum meter seed disk is about to rotate, the seeds to be adsorbed near the surface of the vacuum meter seed disk form a stable accumulation state under the action

of gravity and the vertical pressure of the seed group [32] which increases the difficulty of adsorbing seeds. As shown in Figure 3, after the vacuum meter seed disk rotates, the grooves between the two seed disk holes will separate the seeds to be picked up, and then the grooves drag the separated seeds into the seed disk hole area. The quasi-adsorbed seeds linger near the seed suction hole with an initial velocity v_0. Then, the vacuum meter system pulls and holds seeds to the holes of the seed disk, and the seeds move in a circular motion with the seeding disc at a linear velocity v. After the seeds enter the clearing area, under the action of the upper and lower scrapers, the filling process of a single seed is completed; when the seeds reach the seeding area, the airflow is blocked, the seeds are separated from the seeding tray and fall into the seed trench through the seed delivery tube. It should be noted that the groove's depth directly affects whether it can smoothly drag the seeds. Assuming that the maize seed is a rigid body with uniform material, taking the quasi-adsorbed single maize seed as the research object, ignoring the friction between the seeds, the mechanical model of the concave groove stably dragging the seed is established, as shown in Figure 4.

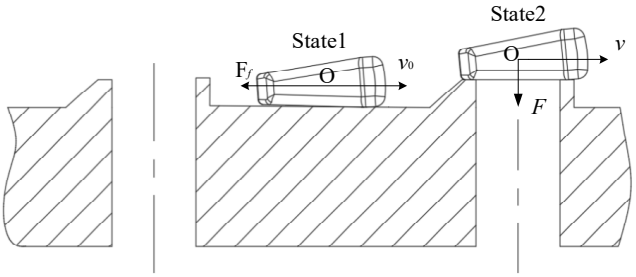

Figure 3. Schematic diagram of groove dragging seed.

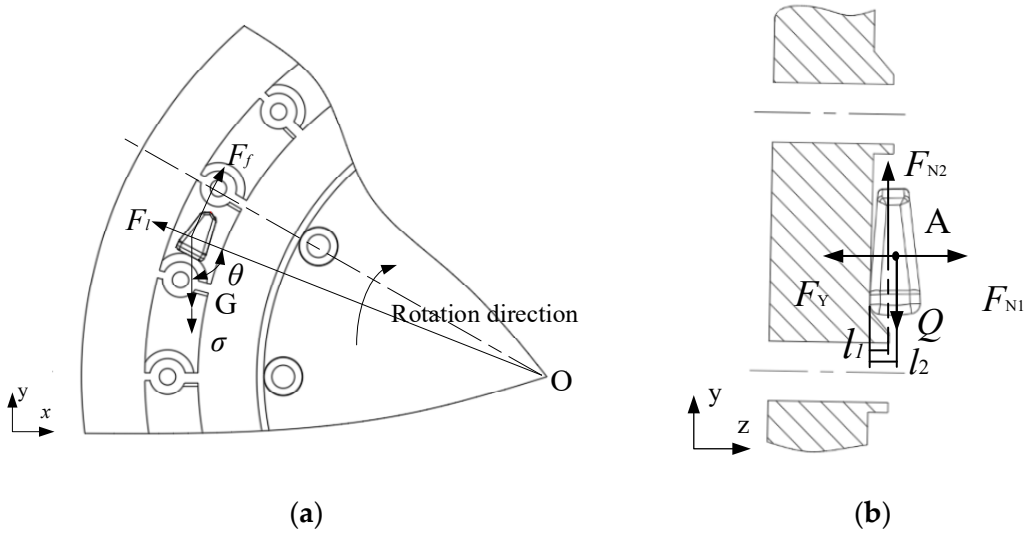

Figure 4. Force analysis of maize seeds in the concave groove. (**a**) *x*–*y* plane; (**b**) *z*–*y* plane.

To make the seed move in the concave groove, it should be satisfied that on the *z*–*y* plane, the rotational torque on the *y*-axis is in a balanced state, as shown in Equation (1):

$$F_{N2}l_1 = Ql_2 \tag{1}$$

where F_{N2} is the supporting force of the concave groove inclined surface to the seed, *N*; Q is the resultant force of the seed on the *y*-axis, *N*; l_1 is the depth of the concave groove, m; l_2 is the distance from the center of mass of the seed to the bottom of the concave groove, m.

$$Q = (G + F_\sigma) - F_l \cos\theta - F_{f1} \sin\theta \tag{2}$$

$$F_\sigma = \gamma h_i S \tag{3}$$

where F_{f1} is the friction between the concave groove and the seed, N; F_l is the inertial centrifugal force, N; G is seed gravity, N; F_σ is the vertical pressure of the upper seed on the lower seed per unit area N; h_i is the distance between the seed layer of the particle and the uppermost seed, m; γ is the weight of the seed, kN/m^3; θ is the angle between centrifugal force and resultant force, °; S is the contact area between the upper seed and the lower seed, m^2.

3. Materials and Methods

3.1. Simulation Parameter Optimization Experiment

3.1.1. Simulation and Optimization Experiment of the Seed Disk Hole

According to previous experiments [9], to solve the problem of high leakage rate when the air-suction seed-metering device works at 8~14 km/h (that is, the speed of the seed metering disc is 18.5 r·min^{-1}–32.5 r·min^{-1}), it is mainly solved by increasing the working pressure to increase the pressure difference of the seed disk hole, thereby increasing the adsorption force. This solution shows that the structure of the seed disk hole affects the velocity and pressure of the airflow in the hole to a certain extent. In this paper, according to the one-dimensional variable cross-section tube steady isentropic flow theory of hydrodynamics [33], as shown in Figure 5, two seed disk holes with different structures were designed based on the original cylindrical seed disk hole structure. Based on the conical seed disk hole, drawing a tangent arc with the straight line EK as the chord length, where the arc is tangent to the straight line QE at point E, an arc with a radius r is obtained, as shown in Figure 5c. The main structural parameters are inlet diameter d_1, outlet diameter d_2 and length L, as shown in Figure 5b,c.

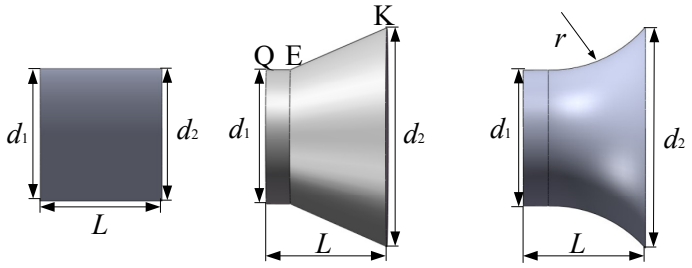

Figure 5. Structure of the seed disk hole: (**a**) cylindrical, (**b**) conical, (**c**) arc.

Because of the different shapes of maize seeds can be divided into horse-tooth shapes, ellipsoid cone shapes and spheroid [34,35]. According to [36], it is known that the air-suction type seed metering device is the most difficult to suck horse-tooth shape maize seeds. From the formula of the diameter of the seed disk hole: d = 0.64 B~0.66 B [37], the average width B of horse-tooth shape seeds is 8.5 mm [35], so it is determined that the diameter d_1 of the inlet of the suction hole is determined to be 5.4~5.6 mm and the cross-sectional area of the seed disk hole entrance is 2.2×10^{-5}~2.5×10^{-5} m^2. The ratio of the velocity at a point in the flow field to the speed of sound at that point is called the local Mach number [38]; the calculation of the Mach number in the one-dimensional pipeline is shown in Equation (4):

$$Ma = \frac{v}{c} \tag{4}$$

where c is the speed of sound, m/s; v is the speed of the gas, m/s.

The previous experiments found that when the air-suction seed-metering device is used to suck seeds under negative pressure, the airflow velocity is less than 80 m/s, and Ma = 0.235 can be calculated. According to the relationship between the internal cross-

sectional area of a one-dimensional pipe and the Mach number in fluid mechanics, from the Isentropic flow aerodynamic function table, it is known that the cross-sectional area ratio of the outlet to the inlet is 2.6 and then the diameter d_2 of the seed disk hole is 8.5~9.1 mm. When high-speed air flows through the pipe, the airflow is also affected by friction. The thickness of the existing vacuum meter seed disk is generally 1.5 mm [37]. Since the depth of the groove is set to be 0.5~2.5 mm in this article, combined with the setting requirements of the orthogonal test parameters, the thickness of the vacuum meter seed disk is 3~7 mm.

The authors used Fluent software to carry out the simulation experiment. The pressure difference between the two sides of the seed disk hole directly determines the ability of the seeding disk to carry seeds stably. So, the pressure difference of the seed disk hole is used as the evaluation index. Combined with theoretical analysis, it can be seen that the form of the seed disk hole and the diameter of the inlet directly determine the size of the pressure difference, thus taking the form of the seed disk hole. Accordingly, an orthogonal experiment was arranged with the inlet diameter d_1 of the seed disk hole and the length L of the seed disk hole as the experimental factors. According to the test results, the influence of the structural parameters of the seed metering device on the performance of the seed metering device was evaluated. In Fluent, the inlet pressure was set to −4 kPa, the angular velocity of the seeding disk was 3 rad/s, and the L9 (3^4) orthogonal experiment table was selected for the simulation experiment. The experimental factors and levels are shown in Table 1 [39].

Table 1. Factors and levels of orthogonal experiments.

Level	Seed Disk Hole Form A	Seed Disk Hole Entrance Diameter d_1/mm	Seed Disk Hole Depth L/mm
1	a	5.4	3
2	b	5.6	5
3	c	5.8	7

3.1.2. Simulation and Optimization Experiment of Groove Depth

According to the analysis in Section 2.2, the grooves between the seed disk holes play an auxiliary role in seed filling. The depth of the groove directly affects the seed filling performance of the vacuum meter seed disk. Therefore, the DEM-CFD coupling method was used to study the effect of the groove depth on the seed filling time and leakage rate under five working speeds and working negative pressures. The level of experimental factors is shown in Table 2.

Table 2. Factor level of experiment.

Level	Groove Depth B/mm	Working Negative Pressure C/kPa	Machine Forward Speed D/km·h^{-1}
1	0.5	2.5	10
2	1	3	11
3	1.5	3.5	12
4	2	4	13
5	2.5	4.5	14

3.1.3. Simulation Model Construction

In this study, Space Claim Direct Modeler (American ANSYS company, which is located in Pittsburgh, PA, USA) was used to establish the fluid domain model of the Vacuum Seed metering device, and ICEM CFD 18.0 (American ANSYS company, which is located in Pittsburgh, PA, USA) was used to draw a hexahedron structured grid of the fluid domain and seed disk hole grid, as shown in Figure 6. The sliding grid method was used to set the seed disk hole as a moving region and set other fluid domains as a static region; the contact surface between the suction hole and the suction chamber, the suction hole and

the seed storage chamber were defined as the interface. The data was transmitted between the moving area and the static area through the interface. The final calculation area had 336,597 grids and the minimum size of the grid model was 1.5×10^{-5} m. The flow field model is shown in Figure 7.

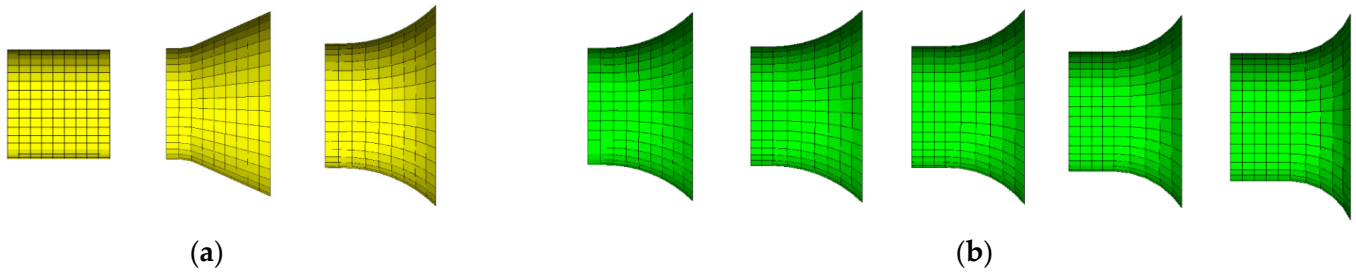

(**a**) (**b**)

Figure 6. Seed disk hole grid: (**a**) Seed disk hole grid with different structures, (**b**) seed disk hole grid with different groove depths.

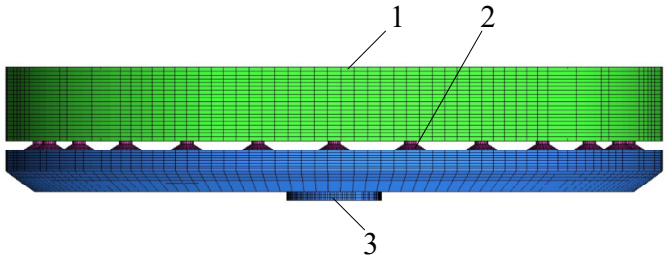

Figure 7. Flow field model: 1. seed storage chamber grid, 2. seed disk hole grid, 3. suction chamber grid.

When the unidirectional airflow was simulated by Fluent, the gas flow was turbulent, and the standard k-ε turbulence model calculated the flow field of the continuous phase. The time step was set to 0.02 s. The number of steps was set to 20,000 steps.

In the DEM-CFD coupled simulation experiment, the Euler–Lagrange method was used, and the ratio of the time step of EDEM (engineering discrete element method) to that of Fluent was between 1:10 and 1:100 [40]. The two software time-step settings must satisfy that the time step in Fluent is an integer multiple of the time step in EDEM, so that the two-way transmission and feedback of data can be realized between the software. Therefore, the time step in EDEM was set to 2×10^{-6}, the time step in Fluent was set to 1×10^{-4}, and the total simulation time was 5 s. The main parameter values required in the simulation experiment [41,42] are shown in Table 3.

Table 3. Simulation parameters.

	Parameter	Maize	Organic Glass
Solid phase	Poisson's ratio	0.4	0.5
	Shear modulus/Pa)	1.37×10^8	1.77×10^8
	Density/kg·m^{-3}	1197	1180
	Restitution coefficient (with seed)	0.182	0.621
	Static friction coefficient (with seed)	0.431	0.459
	Rolling friction coefficient (with seed)	0.0782	0.0931
Gas phase	Fluid	Air	
	Gravitational acceleration/m·s^{-2}	9.81	
	Density/kg·m^{-3}	1.225	
	Dynamic viscosity/Pa·s	1.7894×10^{-5}	

3.1.4. Seed Model Construction

In the process of DEM-CFD coupling, in order to avoid the distortion of flow field calculation, it is necessary to ensure that the particle volume is smaller than the grid volume.

In this article, the maize seed model was established by the Hertz–Mindlin Bonding model and API particle replacement method in EDEM. In the simulation, the Zhengdan958 horse-tooth maize seed was chosen as the modeling object for the simulation particle. First, SolidWorks was used to draw the three-dimensional model of corn seeds and then used the cohesive particle model and particle replacement method in the EDEM software to obtain the corn seed model required for simulation. As shown in Figure 8, from left to right in the figure are the seed physical map, the three-dimensional model map and the particle bonding model map. In the simulation, according to the above method, 300 corn seeds were generated in the pellet factory.

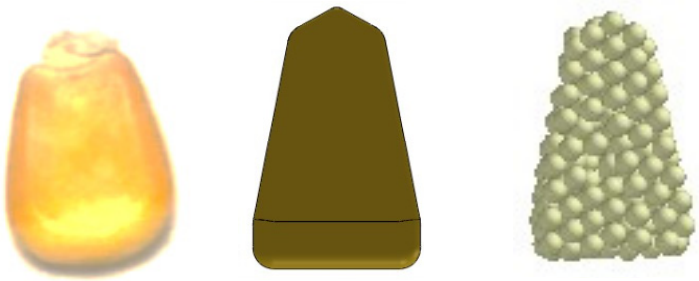

Figure 8. Maize seed simulation model.

3.1.5. Seed Model Construction

In the initial working stage, the Vacuum Seed metering device relies on airflow to stably suck single seeds from the dense seed group, which belongs to the dense phase particle flow system [43]. In the gas–solid coupling simulation, EDEM adopts the coupling interface mainly based on drag force and buoyancy force. When the volume of seeds in the filling area accounts for more than 30%, the seeds cannot be adsorbed under the same working conditions as the real test. In order to improve the simulation accuracy, the calculation of the pressure gradient force needs to be added to the coupling interface [44]. The pressure gradient force is shown in Equation (5):

$$F_P = -V_P dp/dx = -V_P(\rho_f g + \rho_f v dv/dx) \quad (5)$$

where F_p is the pressure gradient force on the particle, N; V_p is the particle volume, m^3; p_f is the gas density, kg/m^3; g is gravitational acceleration, m/s^2; v is the speed of the gas, m/s; d_p/d_x is pressure gradient in a certain direction.

3.2. Bench Experiment

The DEM-CFD coupling method was used to optimize the structure of the disturbance-assisted Vacuum Seed metering device. To verify the accuracy of the optimization of the DEM-CFD coupling method, a bench experiment was carried out between the optimized seed metering device and the original one. The experiment used 3D printing to produce a conical seed disk hole with a groove depth of 1.5 mm. Zhengdan 958 horse-tooth maize seeds were selected, with a moisture content of 13% and a thousand-grain mass of 375 g. Taking the working negative pressure and the working speed as experimental factors and the leakage rate, multiple rate and qualified rate as evaluation indexes, the experiment was carried out on the 2PST planting experiment bench of the Chinese Academy of Agricultural Mechanization, as shown in Figure 9.

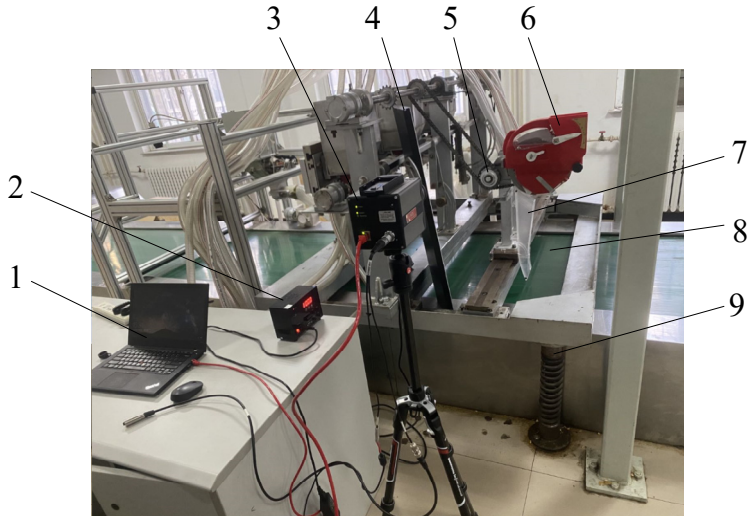

Figure 9. Test bench: 1. computer, 2. light source controller, 3. L-PRI 1000 high-speed camera (produced by AOS Technologies AG, with a frame rate of 500 frames per second during the test), 4. light source, 5. driving device, 6. Vacuum Seed metering device, 7. seed guide tube, 8. seed bed belt, 9. vibration device.

3.3. Experimental Index Calculation Method

In total, 120 seed disk holes were selected to calculate the number of leakage rate, as shown in Equation (6):

$$\begin{cases} y_1 = \frac{n_1}{N} \times 100\% \\ y_2 = \frac{n_2}{N} \times 100\% \\ y_3 = \frac{n_3}{N} \times 100\% \end{cases} \quad (6)$$

where y_1 is the leakage rate, %; y_2 is the multiple rate, %; y_3 is the qualified rate, %; n_1 is the number of holes; n_2 is the number of multi-seed holes; n_3 is the number of single-seed holes; N is the number of theoretical seeding hole.

The time interval from the particles that were not adsorbed to stably picked up indirectly reflects the filling performance of the seeding tray. Fifty seeds were selected to calculate the average picking-up time, as shown in Equation (7).

$$\begin{cases} t_i = t_2 - t_1 \\ y_4 = \frac{\sum_{i=1}^{50} t_i}{50} \end{cases} \quad (7)$$

where t_1 is the moment when the angular velocity of the seed is zero, s; t_2 is the moment when the angular velocity of the seed is the same as the angular velocity of the seeding disk, s; t_i is the picking-up time of a single seed, s.

3.4. Data Statistical Method

IBM SPSS Statistics 19 software (International Business Machines Corporation, which is located in Armonk, NY, USA) was used to analyze the variance of the experimental data, and the F test was used to judge the regression effect of the regression model, that is, to test whether the changes of the experimental factors have a significant impact on the observed values of the experimental results. In the analysis of variance table, the main reference is the significance (p) to analyze the significance of the influence of each factor on the index.

4. Experimental Results and Discussion

4.1. Influence of the Seed Disk Holes on Air Pressure

4.1.1. Analysis of Orthogonal Experimental Results

The results of the orthogonal experiment are shown in Table 4. The general linear regression analysis of the experimental data is carried out by using SPSS software (International Business Machines Corporation, which is located in Armonk, NY, USA), th; theults of analysis of variance are shown in Table 5. The analysis of variance showed that the form, entrance diameter and length of the seed disk hole had significant effects on the dynamic pressure of the seed disk hole ($p < 0.05$). The influence of various factors on the average pressure difference of the seed disk hole is in the following order: the form of the seed disk hole > the entrance diameter of the seed disk hole > the length of the seed disk hole. The larger the suction hole's average pressure difference, the better. Through the analysis of the experimental results, it is known that the optimal structure of the seed disk hole is an arc-shaped seed disk hole, the entrance diameter is 5.4 mm, and the length is 5 mm.

Table 4. Orthogonal experimental results.

No.	Seed Disk Hole Form A	Seed Disk Hole Entrance Diameter d_1/mm	Seed Disk Hole Depth L/mm	Average Difference of Seed Disk Hole Pressure/Pa
1	a	5.4	3	1031
2	a	5.5	5	926
3	a	5.6	7	769
4	b	5.4	5	1391
5	b	5.5	7	1484
6	b	5.6	3	1169
7	c	5.4	7	1742
8	c	5.5	3	1536
9	c	5.6	5	1604
Average difference of seed disk hole pressure	k_1 908.6	1388	1245.33	
	k_2 1384	1315.33	1307	
	k_3 1627.3	1180.67	1331.67	
	R 718.67	207.33	86.34	

Table 5. Variance analysis of experiment results.

Source of Variance	Sum of Square	Degree of Freedom	Mean Square	F	p	Sig.
A	804,077.56	2	402,038.78	3337.96	0.0003	**
d_1	263,901.56	2	131,950.78	1095.53	0.001	**
L	8472.22	2	4236.11	35.17	0.028	*
Error	240.89	2	120.44			
Total	19,034,511	8				

Note: ** highly significant; * significant.

4.1.2. Influence of Seed Suction Structure on Air Pressure and Velocity

In terms of the conical-shaped, arc-shaped, one-dimensional variable section tube, as shown in Figure 10, it is assumed that the airflow travels in the x direction of the seed disk hole axis and the average velocity is v. When p is the average pressure on the cross-section perpendicular to the x-axis, Equation (8) can be obtained from the one-dimensional steady-flow Euler equation of motion.

$$\frac{1}{\rho_f} = -v\frac{dv}{dP} \tag{8}$$

By differentiating Equation (8) and dividing it by ρvA, we can obtain Equation (9).

$$\frac{d\rho}{\rho} + \frac{dv}{v} + \frac{dA}{A} = 0 \tag{9}$$

where A is the area of the section perpendicular to the x-axis, m^2; ρ_f is the gas density, kg/m3; v is the speed of the gas, m/s.

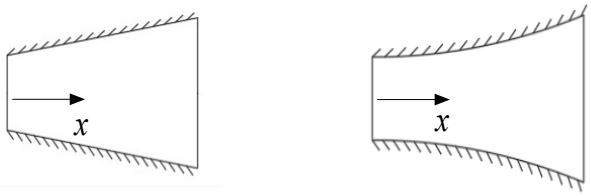

(**a**) (**b**)

Figure 10. Form of one-dimensional variable cross-section tube. (**a**) Conical; (**b**) arc.

Combining Equations (8) and (9) with the sound speed equation $c^2 = dp/d\rho$, we can obtain Equation (10).

$$\frac{dA}{A} = (\frac{v^2}{c^2} - 1)(-\frac{dp}{\rho})\frac{1}{v^2} \tag{10}$$

where c is the speed of sound, m/s.

The experimental results showed that when the suction seed metering device was used to suck seeds under negative pressure, the airflow velocity was less than 80 m/s, which belongs to subsonic flow, so $v^2/c^2 - 1 < 0$. When the inlet diameter of the seed disk hole and the vacuum degree of the suction chamber are the same as those of the original cylindrical seed disk hole, when the seed disk hole adopts the expansion tube structure ($dA > 0$), the airflow flowing through the seed disk hole will decelerate ($dv < 0$) and increase pressure ($dp > 0$).

When the inlet diameter of the seed disk hole is 5.4 mm, and the length is 5 mm, the air pressure and velocity of the seed disk hole with different structures are shown in Figures 11 and 12, respectively. It can be found that the pressure distribution at the inlet of the suction hole is the same; after the airflow through the suction hole, the pressure decreases sharply, the velocity increases, and the pressure is the smallest at the outlet of the suction hole. Among the three shapes of the seed disk holes, the pressure distribution of the cylindrical and arc shapes is uniform, and the pressure distribution of the conical shape is not uniform. The average pressure difference between the inlet and outlet of the seed disk hole is from small to large: cylindrical, conical, arc. The more uniform the pressure distribution of the airflow in the seed disk hole, the greater the pressure difference and the better the adsorption effect on the seeds. Therefore, the structure of the arc-shaped seed disk hole is optimal.

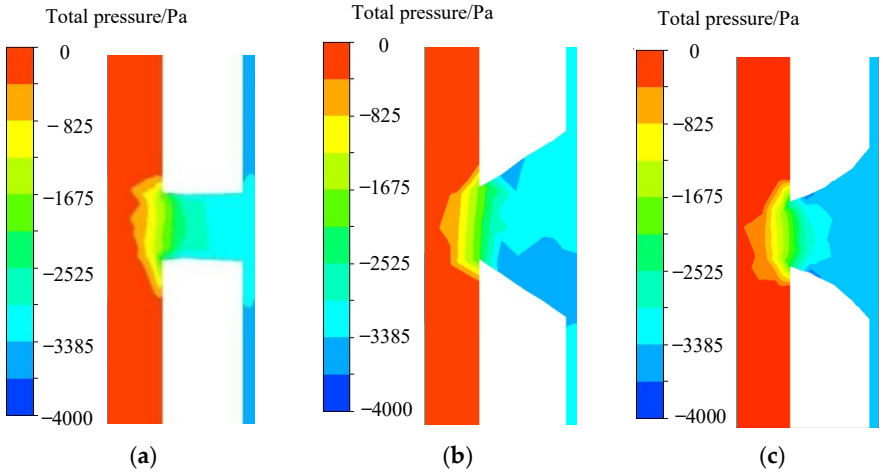

(**a**) (**b**) (**c**)

Figure 11. Air pressure contours of different structures of the seed disk holes. (**a**) Cylindrical; (**b**) conical; (**c**) arc.

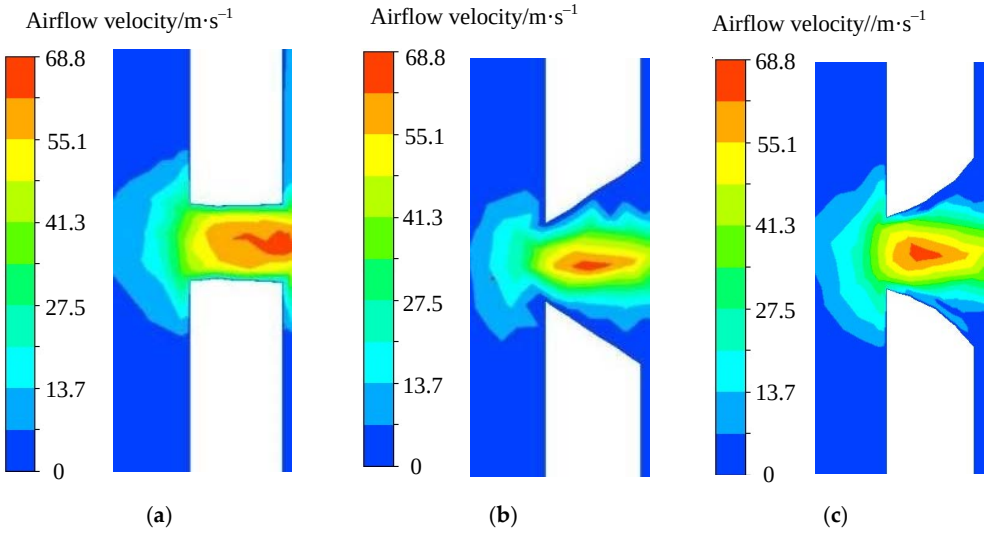

Figure 12. Air velocity contours of different structures of the seed disk holes. (**a**) cylindrical; (**b**) conical; (**c**) arc.

4.1.3. Influence of Inlet Diameter of the Seed Disk Hole on Airflow Pressure and Velocity

When the seed disk hole is arc-shaped, and the length is 5 mm, the air pressure and velocity of different inlet diameters are shown in Figure 13. As the diameter of the inlet of the seed disk hole increases gradually, the value of the inlet pressure increases, and the value of the outlet pressure decreases, resulting in the average pressure difference between the outlet and the inlet of result in decreases. When the diameter is 5.4 mm, the average pressure difference of the suction hole is the largest. Therefore, the inlet diameter of the seed disk hole should be chosen as 5.4 mm.

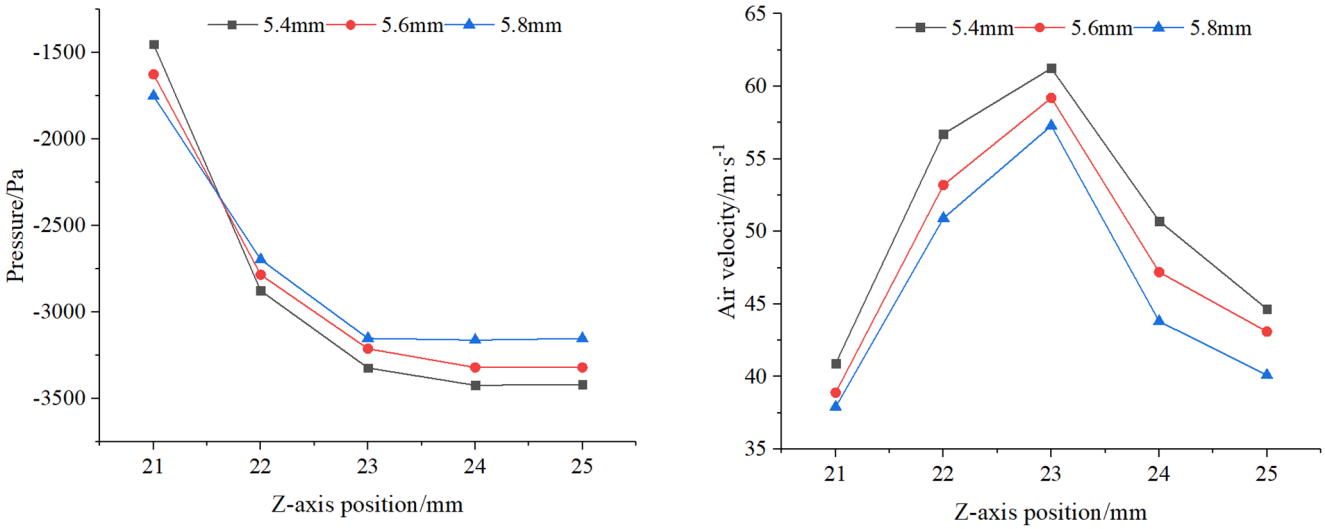

Figure 13. Air pressure and velocity at different inlet diameters of the seed disk holes.

4.1.4. Influence of the Seed Disk Hole Length on Average Pressure Difference

When the seed disk hole is arc-shaped, and the inlet diameter is 5.4 mm, the average pressure difference under different lengths of the seed disk hole is shown in Figure 14. With the increase of the seed disk hole length, the change of average pressure difference is small.

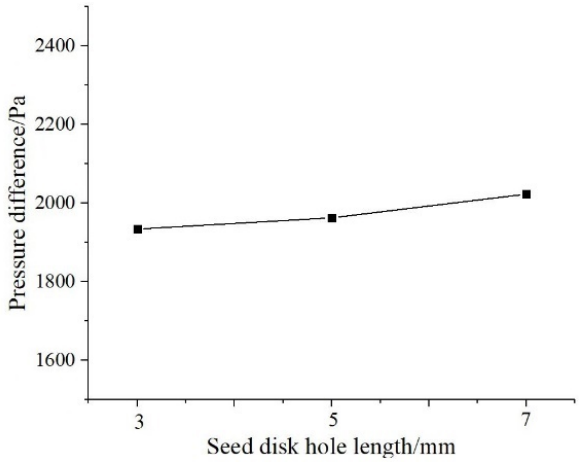

Figure 14. Influence of the seed disk hole length on the average pressure difference.

4.2. Influence of Groove Depth on Leakage Rate

In order to explore the influence of groove depth on the working performance of the seed metering device, Figure 15a shows the leakage rate of the seed metering device when the working speed is 12 km·h^{-1}, the working negative pressure is 2.5~4.5 kPa, and the groove depth is 0.5~2.5 mm. Figure 15b shows the leakage rate of the seed metering device when the working negative pressure is 4 kPa, the working speed is 10~12 km·h^{-1}, and the groove depth is 0.5~2.5 mm. Figure 16 shows the dynamic simulation process of the seed metering device adsorbing seeds under different groove depths. It can be seen from Figure 15a that when the working speed is constant and the working negative pressure is 2.5 kPa, the leakage rate decreases first and then increases with the increase of the groove depth. In combination with Figure 16a, we can see that the upper seed group has a greater pressure on the lower seed group when the groove depth is small; the vacuum meter seed disk cannot effectively disturb and drag the seeds, which are near the surface of the metering disk. As the working negative pressure increases, the leakage rate decreases. When the groove depth is 2~2.5 mm, the leakage rate is relatively large at each working negative pressure level. Combined with Figure 16c, it is found that when the groove depth is too large, under the extrusion of the same layer seed group and the dragging of the high-speed rotating vacuum meter seed disk, the seeds cannot smoothly enter the seed disk hole area, but will be stuck in the grooves, resulting in the phenomenon of a stuck seed. When the working negative pressure increases, the seed disk holes will suck other particles from the nearby seed disk holes. The leakage rate is decreasing.

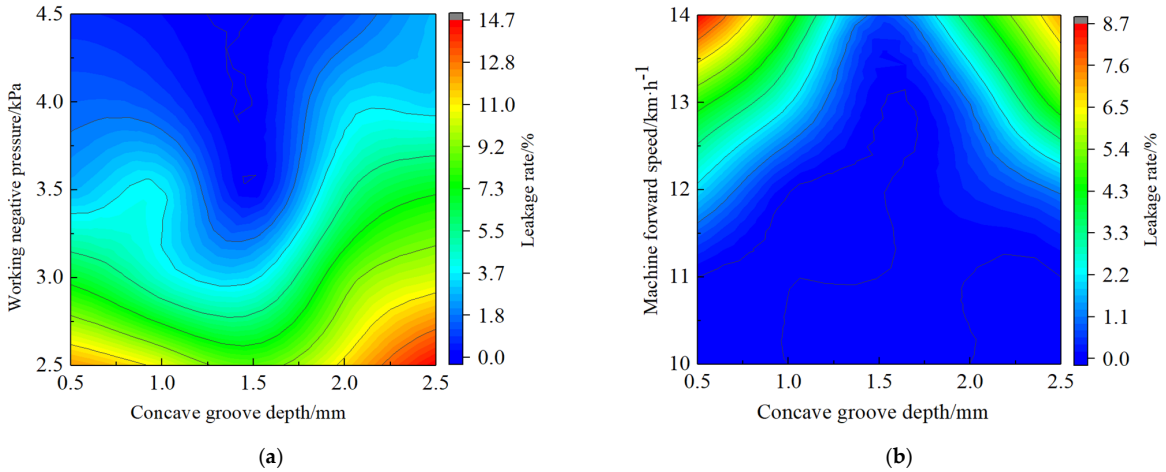

Figure 15. Influence of two-factor interaction on the leakage rate. (**a**) The machine's forward speed is 12 km·h^{-1}, (**b**) the working negative pressure is 4 kPa.

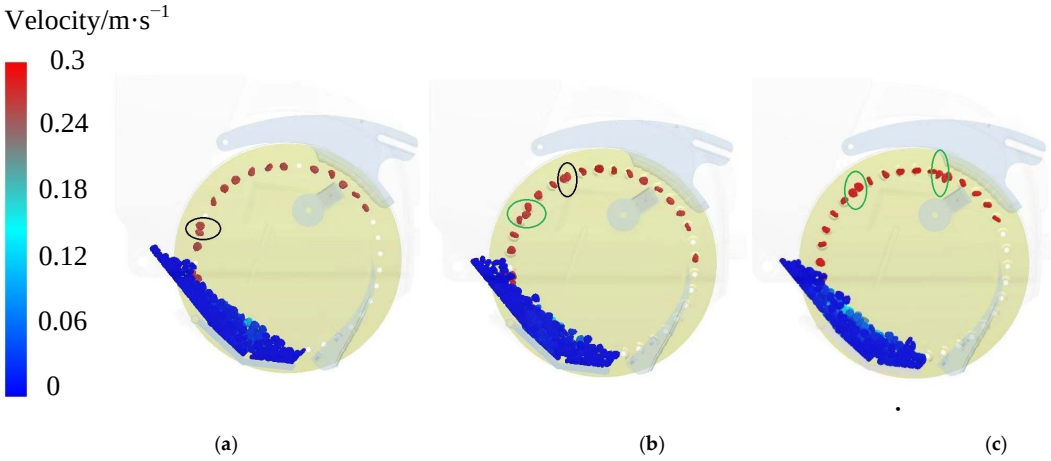

Figure 16. Dynamic simulation process of the seed metering device sucking seeds under different groove depths. (**a**) 0.5 mm, (**b**) 1.5 mm, (**c**) 2.5 mm. Note: The black circle represents the sucked multiple seeds, and the green circle represents stuck seeds.

It can seen from Figure 16b that with the working negative pressure is 4 kPa as a fixed factor, when the forward speed of the machine is less than 12 km·h^{-1}, the leakage rate of the seed metering device is all lower. When the groove depth is 0.5~1 mm and 2~2.5 mm, with the increase of the forward speed of the machine, the leakage rate increases. To sum up, it can be seen the groove depth should be chosen as 1.5 mm.

4.3. Influence of Groove Depth on Picking up Time

To further analyze the working influence of groove depth on the performance of the seed metering device, as shown in Figure 17, when the working speed is 12 km·h^{-1}, the average pinking up time of seeds is plotted under different working negative pressures and groove depths. It can be observed that when the groove depth is a certain value, and the working negative pressure is small, the seed picking-up time is long, as when the working negative pressure increases, the seed picking-up time is short. When the groove depth increases sequentially within 0.5~1.5 mm, the picking-up time is gradually shortened under each negative working negative pressure level. When the groove depth increases sequentially within 1.5~2.5 mm under each working negative pressure level, the picking-up time is gradually increased. When the groove depth is 1.5 mm, the picking-up time is shorter at each working negative pressure level. Therefore, the optimal groove depth should be designed to be 1.5 mm.

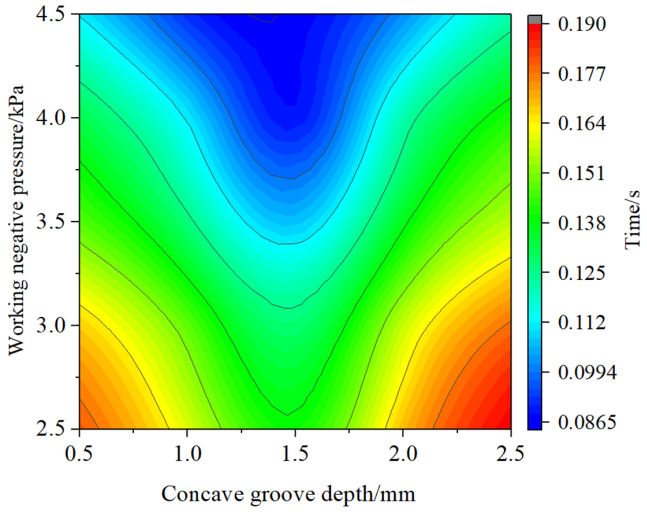

Figure 17. Influence of two-factor interaction on the seed picking-up time.

4.4. Bench Experimental Results

4.4.1. Comparison of Experimental Results

When the forward speed of the seeder is 12 km·h$^{-1,}$ and the working negative pressure of the fan is 2.5~4.5 kPa, the work effect comparison between the optimized seed metering device and the original one is shown in Figure 18. It can be seen from Figure 18a that the leakage rate of the optimized seed metering device is significantly lower than that of the original one within the experimental value range. It can be seen from Figure 18b that the multiple rates of the two seed metering devices are basically the same. As can be observed from Figure 18c, when the working negative pressure is 4~4.5 kPa, the qualified rate of the optimized vacuum seed meter is not less than 96.48%, and the qualified rate of the optimized vacuum seed meter is more than 91%. Therefore, the qualified rate of seed filling of the original seed metering device is obviously lower than that of the optimized rate. This indicates that the optimized seed metering device was used. It is beneficial to increase the qualified rate of filling seeds.

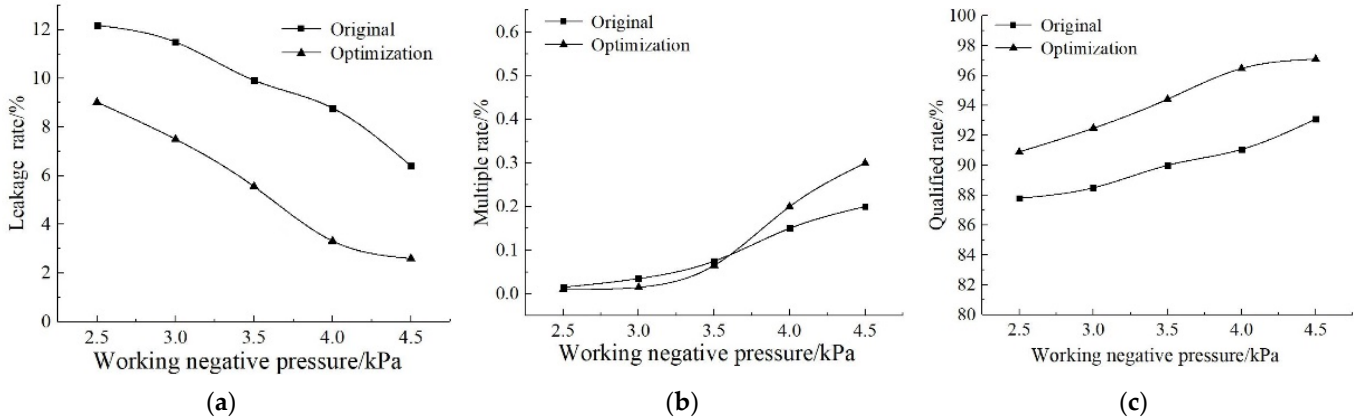

Figure 18. Comparison of the working performance of the seed metering device. (**a**) Lcakage rate; (**b**) Multiple rate; (**c**) Qualified rate.

4.4.2. Working Performance

When working in the field, the vibration will affect the working performance of the vacuum seed meter. To be close to the actual operation, according to the vibration data collected in [29], the operation performance test of the optimized seed meter was carried out under the simulation of normal working conditions. The working negative pressure of the experimental parameters was 4 kPa, and the working speed was selected as 8, 10, 12 and 14 km/h. The rotational speed of the seed disk was calculated with the theoretical grain distance of 20 cm. Three groups of experiments were repeated each time. The test results are shown in Table 6.

Table 6. Experimental results.

Vibrating Frequency/Hz	Speed/km·h^{-1}	Leakage Rate/%	Multiple Rate/%	Qualified Rate/%
2.7	8	0.8	2.2	97.1
4.4	10	1.9	1.7	96.4
7.1	12	3.2	1.1	95.7
9.5	14	4.6	0.4	95.0

To further explore the working performance of the optimized seed-metering device, a single factor test was carried out with the working negative pressure as 4 kPa and the forward speed of the machine as 8~14 km·h^{-1}. The test results are shown in Table 6. The test results show that at each speed level, the qualified rate of the seed metering device is more than 95%, the leakage rate is not more than 4.6%, and the multiple rate is less than 2.2%. All the test indicators showed better results than the national standard requires.

5. Discussion

Through the analysis of the average pressure difference of the seed disk holes, it is shown that as the diameter of the seed disk hole gradually increases, the average pressure difference of the seed disk holes decreases; when the seed disk holes are arc-shaped, the average pressure difference of the seed disk holes is the largest. It is proven that optimizing the seed disk hole can improve the working performance of the vacuum seed meter. In our analysis of the changes in the leakage rate and picking-up time under different groove depths, the working principle of the seed metering device was also analyzed from the perspective of the movement of adsorbed seeds. It shows that the groove has the function of auxiliary seed filling.

The comparative test results show that under the same working negative pressure, the optimized seed metering device can effectively suck seeds and reduce the leakage rate of seeds and the energy consumption of fans. The working performance experiments show that the optimized vacuum seed meter can measure individual seeds well from a seed hopper under real field conditions and sequentially deliver them to a seed delivery tube. The research results of this paper can provide a new design idea for optimizing the structure of air suction in a seed metering device and meeting the requirements of a high-speed sowing operation.

6. Conclusions

In this paper, the Fluent numerical analysis method was used to simulate the influence of the shape, inlet diameter, and length of the suction hole on the airflow field. In addition, the DEM-CFD coupling method was used to explore the effects of groove depth, working negative pressure and seeder forward speed on the working performance of the seed metering device, leading to the following conclusions were obtained:

(a) The shape, inlet diameter and length of the seed disk hole had important effects on the airflow field. Increasing the inlet diameter of the seed disk hole led to a decrease in pressure difference within a certain range, and the seeds were not easily adsorbed. The length of the seed disk hole had little effect on the pressure difference. The structure of the arc-shaped seed disk hole was better, and the pressure difference of the seed disk hole was the largest. We conclude that when the seed disk hole adopts the structure of the expansion tube, the airflow through the seed disk hole can increase the pressure difference and then reduce the fan's energy consumption.

(b) The depth of the groove has an important influence on the process of sucking seeds. When the depth of the groove was large, the seeds easily became stuck in the grooves, resulting in the phenomenon of the stuck seed. When the depth of the groove is small, the seed cannot be dragged; the auxiliary filling effect cannot be achieved. When the groove depth was 1.5 mm, the seed could be dragged smoothly, and the auxiliary filling effect was better.

(c) The bench experiments proved that the DEM-CFD model can accurately evaluate the performance of the seed metering device as a reliable tool for the optimization of the seed meter. The qualified rate of the optimized seed metering device could reach 95% when the working negative pressure was 4 kPa, and the operating speed was 8~14 km·h^{-1}, with a good seed-filling performance. When the working parameters were the same, the qualified rate of the seed metering device designed in this article was increased by 3.4% compared with the vacuum seed metering device developed in [32]. In future, the effect of seed adsorption posture on the seeding process will be studied so the vacuum seed metering device can be better applied in actual production.

Author Contributions: Conceptualization, J.Z. and L.L.; methodology, R.L.; software, R.L.; validation, Q.L.; formal analysis, R.L.; investigation, Z.L. and R.L.; resources, Z.L. and L.L.; data curation, R.L. and J.Z.; writing—original draft preparation, R.L.; writing—review and editing, J.Z. and L.L.; visualization, Q.L. and R.L.; supervision, Y.L. and Z.L.; project administration, Z.L. and L.L.; funding acquisition, L.L. and Z.L. All authors have read and agreed to the published version of the manuscript.

Funding: This work was mainly supported by the Major Science and Technology Special Task Plan of China Machinery Industry Corporation Limited (ZDZX2020-2).

Institutional Review Board Statement: Not applicable.

Informed Consent Statement: Not applicable.

Data Availability Statement: Data are contained within the article. The data presented in this study can be requested from the authors.

Conflicts of Interest: The authors declare no conflict of interest.

References

1. Ding, L. Design and Experimental Study of High-Speed Precision Seed-Metering Device with Auxiliary Seed-Filling and Air-Suction. Ph.D. Thesis, China Agricultural University, Beijing, China, 2020. (In Chinese with English Abstract).
2. Shi, S. Design and Experimental Research of the Pneumatic Maize Precision Seed-Metering Device with Combined Holes. Ph.D. Thesis, China Agricultural University, Beijing, China, 2020. (In Chinese with English Abstract).
3. Liao, Q.X.; Huang, H.D.; Wu, F.T. The situation and the prospect of corn precision metering mechanization in China. *Agric. Equip. Technol.* **2006**, *1*, 4–7. (In Chinese with English Abstract)
4. Zhang, D. *Technology and Equipment for Mechanized Maize Production*; China Agricultural University Press: Beijing, China, 2014. (In Chinese with English Abstract)
5. Li, Y.H. Optimal Design and Experimental Study of Cleaning and Linear Throwing Mechanism of the High-Speed Maize Precision Seed-Metering Device. Ph.D. Thesis, China Agricultural University, Beijing, China, 2021. (In Chinese with English Abstract).
6. Fu, W.Q. Study on Key Technology of Quality Control for Maize No-Tillage Drilling Machinery. Ph.D. Thesis, China Agricultural University, Beijing, China, 2018. (In Chinese with English Abstract)
7. Yang, L.; Yan, B.X.; Zhang, D.X.; Zhang, T.L.; Wang, Y.X.; Cui, T. Research progress on precision planting technology of maize. *Trans. Chin. Soc. Agric. Mach.* **2016**, *47*, 38–48. (In Chinese with English Abstract)
8. Lai, Q.H.; Zhao, J.W.; Su, W.; Jia, G.X.; Li, J.H.; Lu, Q. Design and test of air suction directional transplanting device for panax notoginseng seeding based on DEM-CFD. *Trans. Chin. Soc. Agric. Mach.* **2021**, *52*, 60–70. (In Chinese with English Abstract)
9. Gao, X.J. Study on Precision Seeding Technology and Device Based on High-Speed Centrifugal Filling-Clearing. Ph.D. Thesis, China Agricultural University, Beijing, China, 2021. (In Chinese with English Abstract)
10. Brosh, T.; Kalman, H.; Levy, A.; Peyron, I.; Ricard, F. DEM-CFD simulation of particle comminution in jet-mill. *Powder Technol.* **2014**, *257*, 104–112. [CrossRef]
11. Lei, X.L.; Liao, Y.T.; Liao, Q.X. Simulation of seed motion in seed feeding device with DEM-CFD coupling approach for rapeseed and wheat. *Comput. Electron. Agric.* **2016**, *131*, 29–39. [CrossRef]
12. Wang, L.; Liao, Y.T.; Wan, X.Y.; Wang, B.S.; Hu, Q.L.; Liao, Q.X. Design and test on mixing component of air-assisted centralized metering device for rapeseed and wheat. *Trans. Chin. Soc. Agric. Mach.* **2022**, *53*, 68–79. (In Chinese with English Abstract)
13. Gao, X.J.; Cui, T.; Zhou, Z.Y.; Yu, Y.B.; Xu, Y.; Zhang, D.X.; Wei, S. DEM study of particle motion in novel high-speed seed metering device. *Adv. Powder Technol.* **2021**, *32*, 1438–1449. [CrossRef]
14. Gao, X.J.; Zhou, Z.Y.; Xu, Y.; Yu, Y.B.; Su, Y.; Cui, T. Numerical simulation of particle motion characteristics in quantitative seed feeding system. *Powder Technol.* **2020**, *367*, 643–658. [CrossRef]
15. Ren, B.; Zhong, W.Q.; Chen, Y.; Chen, X.; Jin, B.S.; Yuan, Z.L.; Lu, Y. CFD-DEM simulation of spouting of corn-shaped particles. *Particuology* **2012**, *10*, 562–572. [CrossRef]
16. Ding, L.; Yang, L.; Wu, D.H.; Li, D.Y.; Zhang, D.X.; Liu, S.R. Simulation and experiment of corn air suction seed metering device based on DEM-CFD coupling method. *Trans. Chin. Soc. Agric. Mach.* **2018**, *49*, 48–57, (In Chinese with English Abstract).
17. Guzman, L.; Chen, Y.; Landry, H. Coupled CFD-DEM simulation of seed flow in an air seeder distributor tube. *Processes* **2020**, *8*, 1597. [CrossRef]
18. Arzu, Y.; Vedat, D.; Adnan, D. Comparison of computational fluid dynamics-based simulations and visualized seed trajectories in different seed tubes. *Turk. J. Agric. For.* **2020**, *44*, 599–611.
19. Pasha, M.; Hassanpour, A.; Ahmadian, H.; Tan, H.S.; Bayly, A.; Ghadiri, M. A comparative analysis of particle tracking in a mixer by discrete element method and positron emission particle tracking. *Powder Technol.* **2015**, *270*, 569–574. [CrossRef]
20. Landry, H.; Thirion, F.; Lague, C.; Roberge, M. Numerical modeling of the flow of organic fertilizers in land application equipment. *Comput. Electron. Agric.* **2006**, *51*, 35–53. [CrossRef]
21. Mori, Y.; Sakai, M. Development of a robust Eulerian-Lagrangian model for the simulation of an industrial solid-fluid system. *Chem. Eng. J.* **2021**, *406*, 126841. [CrossRef]
22. Pei, C.L.; Wu, C.Y.; England, D.E.; Byard, S.; Berchtold, H.; Adams, M. DEM-CFD modeling of particle systems with long-range electrostatic interactions. *AIChE J.* **2015**, *61*, 1792–1803. [CrossRef]
23. Jiang, Z.H.; Rai, K.T.; Tsuji, T.; Washino, K.; Tanaka, T.; Oshitani, J. Upscaled DEM-CFD model for vibrated fluidized bed based on particle-scale similarities. *Adv. Powder Technol.* **2020**, *31*, 4598–4618. [CrossRef]
24. Ueda, S.; Kon, T.; Kurosawa, H.; Natsui, S.; Ariyama, T.; Nogami, H. Influence of shape of cohesive zone on gas flow and permeability in the blast furnace analyzed by DEM-CFD model. *ISIJ Int.* **2015**, *55*, 1232–1236. [CrossRef]

25. Di Renzo, A.; Di Maio, F.P. Homogeneous and bubbling fluidization regimes in DEM-CFD simulations: Hydrodynamic stability of gas and liquid fluidized beds. *Chem. Eng. Sci.* **2007**, *62*, 116–130. [CrossRef]
26. Takabatake, K.; Sakai, M. Flexible discretization technique for DEM-CFD simulations including thin walls. *Adv. Powder Technol.* **2020**, *31*, 1825–1837. [CrossRef]
27. Liu, S.J.; Li, Y.W.; Hu, X.Z. Effect of particle volume fraction on the performance of deep-sea mining electric lifting pump based on DEM-CFD. *J. Mech. Eng.* **2020**, *56*, 257–264. (In Chinese with English Abstract)
28. Natsui, S.; Ueda, S.; Nogami, H.; Kano, J.; Inoue, R.; Ariyama, T. Analysis on non-uniform gas flow in blast furnace based on DEM-CFD combined model. *Steel Res. Int.* **2011**, *82*, 964–971. [CrossRef]
29. Shi, S.; Liu, H.; Wei, J.G.; Zhou, J.L.; Jian, S.C.; Zhang, R.F. Optimization and experiment of pneumatic seed metering device with guided assistant filling based on EDEM-CFD. *Trans. Chin. Soc. Agric. Mach.* **2020**, *51*, 54–66. (In Chinese with English Abstract)
30. Ding, L.; Yang, L.; Zhang, D.X.; Cui, T.; Zhang, K.; Zhong, X. Effect of seed adsorption posture of corn air-suction metering device on seed feeding performance. *Trans. Chin. Soc. Agric. Mach.* **2021**, *52*, 40–50. (In Chinese with English Abstract)
31. Han, D.D.; Zhang, D.X.; Jing, H.R.; Cui, T. DEM-CFD coupling simulation and optimization of inside-filling air-blowing maize precision seed-metering device. *Comput. Electron. Agric.* **2018**, *150*, 426–438. [CrossRef]
32. Yang, M.Z. *Rheology of Agricultural Materials*; China Agriculture Press: Beijing, China, 2015. (In Chinese with English Abstract)
33. Ding, R.Z. *Fluid Mechanics*; Higher Education Press: Beijing, China, 2018; (In Chinese with English Abstract).
34. Chen, Z.R.; Yu, J.Q.; Xue, D.M.; Wang, Y.; Zhang, Q.; Ren, L.Q. An approach to and validation of maize-seed-assembly modelling based on the discrete element method. *Powder Technol.* **2018**, *328*, 167–183. [CrossRef]
35. Zhou, L.; Yu, J.Q.; Wang, Y.; Yan, D.X.; Yu, Y.J. A study on the modelling method of maize-seed particles based on the discrete element method. *Powder Technol.* **2020**, *347*, 353–376. [CrossRef]
36. Ding, L.; Yang, L.; Zhang, D.X.; Cui, T.; Gao, X.J. Design and experiment of vacuum meter seed disk of corn air suction seed metering device based on DEM-CFD. *Trans. Chin. Soc. Agric. Mach.* **2019**, *50*, 50–60. (In Chinese with English Abstract)
37. Chinese Academy of Agricultural Mechanization Sciences. *Handbook of Agricultural Machinery Design*; Machinery Industry Press: Beijing, China, 2007; pp. 343–347, (In Chinese with English Abstract).
38. Pan, J. The Large-Time Behavior of the Compressible Fluid in 1-D and the Stability of the of the Boundary Layer of the Non-Newtonian Fluid. Master's Thesis, Northwest University, Xi'an, China, 2012. (In Chinese with English Abstract)
39. Yuan, Z.F.; Zhou, J.Y. *Experimental Design and Analysis*; Higher Education Press: Beijing, China, 2000; pp. 112–118. (In Chinese with English Abstract)
40. Liu, Z.D.; Wang, Q.J.; Li, H.W.; He, J.; Lu, C.Y. Fertilizer injecting route analysis and test for air-blowing seed-fertilizer hole-applicator via CFD-DEM coupling. *Trans. Chin. Soc. Agric. Eng.* **2019**, *35*, 18–25. (In Chinese with English Abstract)
41. Cui, T.; Liu, J.; Yang, L.; Zhang, D.X.; Zhang, R.; Lan, W. Experiment and simulation of rolling friction characteristic of corn seed based on high-speed photography. *Trans. Chin. Soc. Agric. Eng.* **2013**, *29*, 34–41. (In Chinese with English Abstract)
42. Wang, Y.X.; Liang, Z.J.; Zhang, D.X.; Cui, T.; Shi, S. Calibration method of contact characteristic parameters for corn seeds based on EDEM. *Trans. Chin. Soc. Agric. Eng.* **2016**, *32*, 36–42. (In Chinese with English Abstract)
43. Li, J.H.; Ou, Y.J.; Gao, S.Q.; Ge, W.; Yang, N.; Song, W. *Multi-Scale Simulation of Particle-Fluid Complex System*; Science Press: Beijing, China, 2005. (In Chinese with English Abstract)
44. Zhu, H.P.; Zhou, Z.Y.; Yang, R.Y.; Yu, A.B. Discrete particle simulation of particulate systems: Theoretical development. *Chem. Eng. Sci.* **2006**, *62*, 3378–3396, (In Chinese English Abstract). [CrossRef]